International Journal of Heat and Mass Transfer 257 (2026) 128248

Contents lists available at ScienceDirect

International Journal of Heat and Mass Transfer

journal homepage: www.elsevier.com/locate/ijhmt

Experimental analysis of operating parameters in membrane humidifiers for fuel cell systems

Sören Tinz [a], Julian Toussaint [b,*], Maximilian Schmitz [a], Marius Walters [a], Stefan Pischinger [b]

[a] FEV Europe GmbH, Neuenhofstr. 181, 52078 Aachen, Germany
[b] Chair of Thermodynamics of Mobile Energy Conversion Systems (TME), RWTH Aachen University, Forckenbeckstr. 4, 52074 Aachen, Germany

ARTICLE INFO

Keywords:
Fuel cell system
Membrane humidifier
Experiment
Gaussian process regression

ABSTRACT

Membrane humidifiers are key components in PEM fuel cell systems (PEMFC), yet their behavior under realistic operating conditions is insufficiently documented, especially for full-scale devices. This work experimentally investigates the influence of major operating parameters on two complete gas-to-gas membrane humidifiers and generates a comprehensive dataset covering relevant fuel-cell (FC) system conditions. Based on these measurements, a Gaussian Process Regression (GPR) correlation model is developed that accurately predicts water transfer and outlet temperatures ($R^2 > 0.99$). The results reveal the dominant role of feed-side mass flow, inlet humidity and permeate temperature on humidifier performance, and show that differential pressure has no measurable effect. From these findings, practical guidelines for humidifier integration and operation in fuel cell systems are derived, such as locating bypasses on the feed side for robust humidity control and efficient drying. These contributions provide a validated basis for improved system simulations and support more reliable and efficient PEM fuel cell system design.

1. Introduction

Proton conductivity in polymer electrolyte membrane fuel cells (PEMFCs) strongly depends on membrane humidity [1]. To ensure high fuel cell (FC) performance, the cathode supply air is therefore humidified in most commercial systems. While some manufacturers, such as Toyota, rely on internal humidification concepts and operation with dry cathode air [2], the majority of passenger-car systems use external humidification upstream of the stack [3,4]. Several concepts have been discussed in the literature, including liquid water injection or cathode exhaust gas recirculation, but membrane humidifiers remain the most widely applied solution.

For system development, a detailed understanding of the humidifier behaviour under realistic operating conditions is essential. The fundamental mechanisms of water transport through polymer electrolyte membranes and hollow-fibre structures are well established, and numerous 0D to 3D modelling approaches have been proposed to describe heat and mass transfer in membrane humidifiers [5–7,12,13,17,23,24,28]. These approaches provide valuable insight into the underlying transport phenomena and the influence of geometric and material parameters. Experimental studies have further contributed to understanding specific aspects of humidifier behaviour, yet they are predominantly performed on single membranes or small-scale test configurations, often under simplified or idealised boundary conditions [7,11,20–22,31]. Typical assumptions include constant membrane temperature, uniform gas properties, or negligible heat losses, which do not reflect the complex thermal–fluid environment of an integrated fuel cell system [5,6,9,16–18,33].

As a result, two central research gaps remain. First, the behaviour of full-scale gas-to-gas membrane humidifiers under realistic fuel-cell-system conditions is still insufficiently understood [7,9,13,15,16,18,20]. Existing experimental datasets cover only limited operating ranges and do not capture the coupled effects of temperature, humidity, pressure, and unequal mass flows that occur in practical operation. Second, current empirical or semi-analytical models are typically validated only against small-scale experiments and therefore fail to reproduce the trends and nonlinear interactions observed in real components, particularly with respect to outlet temperatures, humidity distributions, and the interplay of feed and permeate conditions [5,9,10,13,17,29,30,32].

The present study addresses these gaps through three key contributions.

* Corresponding author.
E-mail address: toussaint@tme.rwth-aachen.de (J. Toussaint).

https://doi.org/10.1016/j.ijheatmasstransfer.2025.128248
Received 30 September 2025; Received in revised form 27 November 2025; Accepted 10 December 2025
Available online 16 December 2025

i. A comprehensive parametric investigation of two commercially relevant gas-to-gas membrane humidifiers is performed, covering realistic fuel-cell-system operating conditions with independent control of mass flow rates, pressures, temperatures, and humidity levels.
ii. Scale effects are systematically analysed by normalising the water-transfer performance to the number of fibres, enabling a direct comparison of humidifier sizes that has not been reported previously.
iii. A data-driven Gaussian Process Regression (GPR) model is developed that accurately predicts water transfer and outlet temperatures across the full operating range, significantly improving upon existing empirical correlations and providing a robust basis for system-level simulations.

These contributions advance the understanding of membrane humidifier behaviour beyond the scope of existing modelling and small-scale studies [18,33,35,36]. For the full-scale hollow-fiber humidifiers examined here, no directly comparable 0D–3D simulation data are available in the literature, particularly not for the specific commercial components tested. This limits the possibility of a one-to-one model comparison and is therefore stated explicitly. They provide experimentally grounded insights relevant for the design, integration, and control of humidifiers in PEMFC systems and support the development of more accurate and predictive system simulation tools.

2. Membrane humidifiers

Membrane humidifiers contain two fluid chambers separated by a membrane. The gas to be humidified flows through one chamber, while the water to be transported across the membrane is provided in the other chamber. The water can be either liquid, as in the originally used water-to-gas humidifiers [5–7], or gaseous in gas-to-gas humidifiers [8], which for practical reasons directly use the moist cathode exhaust gas and are the preferred application for mobile use cases and are considered in the following.

The integration of the membrane humidifier is depicted in Fig. 1. The fluid flow providing the water is referred to as feed, the one receiving the water as permeate flow.

The membranes used in humidifiers consist of the same materials as those in fuel cells, e.g. Nafion 212, which was considered the industry standard for a long time but is more and more being replaced by cheaper products [9,10]. One alternative is a composite structure, <5 µm thick, which provides good water transport while reliably separating the gases. In this compound, the mechanical stability is ensured by double-sided microporous layers [11].

One configuration is a hollow-fiber membrane humidifier, in which one fluid stream flows though the interior of a round membrane tube, whereas the other fluid flows along the outside of the tubes [12]. An alternative are plate-and-frame membrane humidifiers, in which the membranes separating the gas chambers are arranged as stacked planes [13]. Analogous to the fuel cell itself, various flow field designs from straight or serpentine channels [14] to sinus- or zig-zag-shaped geometries [15] to porous media in form of metal foams are considered [16]. In both configurations the fluids can be in cocurrent or countercurrent, but also in crosscurrent flow [11,17]. The countercurrent flow leads to a significantly better performance than the cocurrent [18,19] and also than the crosscurrent flow [11,20].

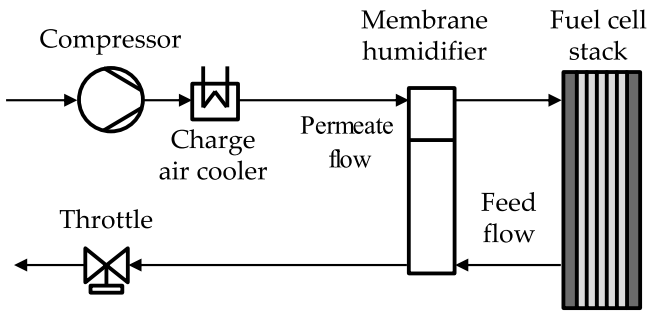

Fig. 1. Air path of a fuel cells system including a membrane humidifier.

Since the same or similar membrane materials are used, the same laws regarding the water content apply to contact humidifiers as in fuel cells themselves. As there is no proton exchange due to the lack of electric potential, electro-osmosis has no basis, and diffusion is the only relevant water transport mechanism through the membrane.

Various characteristic values are used to evaluate membrane humidifier performance and are introduced in the following.

The absolute water transfer $\dot{m}_{H_2O,transfer}$ as a measure is well suited to compare different humidifiers under the same operating conditions. However, an evaluation of the humidifier performance as such is not possible because the water supply and therefore the maximum possible water transfer are not taken into account [21,22]The relative humidity φ or the dew point temperature $T_{\tau,permeate,out}$ at the permeate outlet also do not take into account the maximum possible water transfer [21]. If precise information on pressure and – in the case of relative humidity – temperature is available, they are excellent measurement variables for specifying and evaluating a condition, e.g. at the fuel cell inlet.

The dew point approach temperature (DPAT) as another performance value is defined as the difference in dew point temperatures between the inlet on the feed ($T_{\tau,feed,in}$) and the outlet on the permeate side ($T_{\tau,permeate,out}$). For an ideal humidifier with perfect heat and mass transfer the DPAT equals zero [22]

$$\mathrm{DPAT} = T_{\tau,feed,in} - T_{\tau,permeate,out} \tag{1}$$

Under otherwise constant operating conditions, a smaller DPAT value means better water transfer. Comparisons of the performance in different operating points can be slightly misleading due to the nonlinear correlation of temperature and saturation pressure [22]. Inferences on the absolute water mass transfer, however, cannot be drawn solely based on the DPAT, because the transferred water mass at a certain DPAT strongly depends on the absolute value of the dew point temperature. To determine the state at the permeate outlet, knowledge about the pressure level at this location as well as the dew point at the feed inlet are necessary.

The water recovery ratio (WRR) takes into account the total water mass flow $\dot{m}_{H_2O,feed,in}$, provided in the feed inlet flow and puts the transferred water mass into relation to it [21].

$$\mathrm{WRR} = \frac{\dot{m}_{H_2O,permeate,out} - \dot{m}_{H_2O,permeate,in}}{\dot{m}_{H_2O,feed,in}} \tag{2}$$

The WRR is a suitable value to characterize membrane humidifiers only with dry fluids at the permeate inlet because otherwise the maximum transferable water mass flow rate is less than $\dot{m}_{H_2O,Feed,in}$ [21]. In common fuel cell applications, the membrane humidifier is supplied with compressed ambient air at temperatures above 50 °C which can be considered dry in good approximation. Compressing and heating humid air from ambient pressure with a temperature $T = 25$ °C and a relative humidity φ = 70 % (as it can be observed in tropical climate), up to a pressure p = 2 bar and temperature $T = 70$ °C, results in a relative humidity φ = 14 %. From more moderate ambient conditions of $T = 15$ °C and φ=40 %, the relative humidity at p = 2 bar and $T = 70$ ° is less than φ=5 %.

$$\varepsilon_{latent} = \frac{\dot{m}_{dr,permeate} \cdot \left(X_{permeate,out} - X_{permeate,in}\right)}{\min\left(\dot{m}_{dr,permeate}; \dot{m}_{dr,feed}\right) \cdot \left(X_{feed,in} - X_{permeate,in}\right)} \tag{3}$$

This inaccuracy is compensated for by the latent effectiveness ε_{latent} [21], by taking into account the water content at the permeate inlet [21] as well as different mass flow rates on the feed and permeate side. ε_{latent} describes the ratio between the transferred and the maximum

transferable water mass flow rate which is reached if either the permeate outlet flow reaches the humidity ratio of the feed inlet flow or the feed outlet flow reaches the humidity ratio of the permeate inlet flow. $\dot{m}_{\mathrm{dr.permeate}}$ and $\dot{m}_{\mathrm{dr.feed}}$ denote the mass flow rate of the dry gas on the permeate or feed side, respectively.

Which of the introduced characteristic values is the most suitable, depends on the target of investigation as illustrated in the following example. While reducing the permeate mass flow rate leads to a higher relative humidity and dew point temperature at the permeate outlet and lower dew point approach temperature at constant parameters, the water recovery ratio and latent effectiveness decrease with the lower transferred water mass flow rate [21].

According to the literature, membrane humidifiers exhibit a not inconsiderable inertia. While no differences in speed are noticeable for small changes of the humidity, desorption is an order of magnitude faster than adsorption for larger changes. Especially with thin membranes, it is not diffusion that limits the speed, but the transition between gas phase and membrane. In case of adsorption, the latter is subject to slow membrane swelling [23,24]. The time until the membrane reaches a stable humidity level can be up to 100–1000 s [25].

Furthermore, the membrane humidifier is a passive component whose humidification performance depends on external operating conditions, which can only be influenced to a limited extent independently of those of the fuel cell. One possibility, however, is the use of a bypass [26]. As humidity measurements involve relatively high cost, a pure feed-forward control is preferable over a closed-loop feedback control [27]. Other sources, – despite a liquid-to-gas humidifier without bypass –, however, favor a closed control loop for higher accuracy, while conceding the low dynamics of the humidity sensors at the same time [10].

There exist a variety of zero- and one-dimensional modeling approaches to predict the water transfer of gas-to-gas membrane humidifiers that are most often based on the empirical correlations described in [6,8,12,28–32]. Even investigations with three-dimensional computational fluid dynamics (3D-CFD), which are used to analyze the influence of channel width, height and length [33] or to estimate the potentials of a metal foam layer instead of the channels [34], are usually based on the common correlations from [28]. Experiments described in the literature to investigate the influence of channel dimensions [35], operating conditions [20,36] or model validation [22], which sometimes use sensors integrated into the channels [21], are usually smaller in scale.

Our own experimental investigations prior to this work have shown that the observed behavior of certain commercially available membrane hollow-fiber membrane humidifiers in gas-to-gas configuration cannot be approximated by the 0D and 1D models from the literature. This is not only about the magnitude of the water transfer, but also about the general trend of the influence of the operating parameters. This may be due to the fact that mass humidifiers are subject to different thermal conditions than the single tube or single plate membranes often used for model validation. Another reason is certainly the membrane material differing from Nafion with often unknown specifications.

For fuel cell system modeling, a detailed description of auxiliary components is inevitable. These include the membrane humidifier as a core component whose behavior depends on various complex, nonlinear heat and mass transfer mechanisms. Against this background, an experimental approach can provide sufficient accuracy. The measurement results are incorporated in a Gaussian Process Regression (GPR) model that calculates the outlet temperatures as well as the water transfer for the operating parameters as input variables. Further information on GPR can be found in the literature [37,38].

3. Experimental setup

The experiments were conducted on a flexible fuel cell stack and component test bench. It can be used for testing stacks, fuel cell system components, FC sub systems and FC systems. The modular concept is introduced in [157]. This article first presents the possibilities for fuel cell stack tests and then the concrete implementation of the humidifier tests.

The test bench, depicted in Fig. 2, is designed for a corresponding nominal stack power in the range from 2 kW to 40 kW. In stack tests, apart from drawing the electric load, the cathode supply air, the anode gas and the coolant are conditioned. For the latter, the desired stack inlet temperature is controlled by mixing the warm, recirculated coolant with the cooler stream from the house cooling system. The coolant flow rate variation via the coolant pump rotational speed allows for controlling the temperature spread across the stack. In order to quickly reach the new set point during load point transitions, the pre-controller estimates the heat to be removed and the necessary coolant flow rate. In order to investigate cold start procedures that require temperatures below the minimum facility coolant temperature (in a concrete application case −32 °C) for demonstration purposes, the cooling circuit was enhanced by an additional vapor-compression refrigerator. In order to optionally avoid cold starts, an apparatus for preheating the coolant and the stack is included in the test bench.

On the anode side, the pressure is controlled by the mass flow rate of fresh hydrogen flowing through a solenoid valve. The standard is a constant overpressure of the anode to the cathode inlet. For fast reactions, the mass flow rate is pre-controlled based on the electric load. The anode gas recirculation blower can either be operated with load-dependent constant rotational speed or controlled to a corresponding mass flow rate set point measured by a Coriolis sensor. The intervals for purge and drain events represent an additional degree of freedom and can be defined individually, e.g. dependent on the load.

The cathode supply air is conditioned in terms of mass flow rate, pressure, temperature and relative humidity:

The pressure control is achieved via two throttles downstream of the test object. The pure feed-forward control of one throttle based on the mass flow rate and the estimated pressure losses across the test object serves to extend the operating range of the other throttle, thus reducing the sensitivity of the system response in the areas of an otherwise almost completely closed throttle. The second throttle is pre- and feed-back controlled. This combination enables the precise control of high mass flow rates at low pressures as well as low mass flow rates at high pressures.

The air temperature at the stack inlet is adjusted by means of a heat exchanger through which a separate heat transfer fluid circuit flows. Here, a multi-cascaded controller is used. First, the mass flow rate and temperature-dependent temperature loss of the air between heat exchanger and test object inlet is estimated, calculating an air temperature set point at the heat exchanger outlet. This temperature is manipulated by a controller based on the measured temperature at the test object inlet. The heat exchanger outlet temperature is adjusted to the set point determined this way by mixing a warm recirculated and a cooled fluid stream. In order to find a compromise between an energy efficient as well as dynamic test bench operation, the heating power in

Fig. 2. Frontal view of the test bench.

this circuit is controlled depending on the thermostat valve position.

The humidity at the cathode inlet is adjusted by mixing a dry and a fully saturated air stream based on the principle described in [39]. With the known temperature of the saturated stream, the mass flow rate is chosen in such a way that it carries the necessary absolute water mass, before being mixed with the remaining dry air stream. The tube walls are heated to T > 120 °C to prevent a reduction of the humidity ratio by condensation. Using a feed-forward control, the humidity can be precisely adjusted to 3 % r.h., the additional feed-back control, which manipulates the mass flow rate distribution based on the humidity measured at the test object inlet enables an accuracy of 1 % r.h. This high accuracy ensures sufficient margins to saturation, making liquid water formation in the feed stream highly unlikely. While local condensation inside the humidifier cannot be fully excluded, it would not persist, as the permeate outlet consistently remains far from saturation and any transient droplets would rapidly re-evaporate due to the large internal membrane surface area.

The electric load is either voltage or current controlled and modularly extendable. Nitrogen flushing allows for test object inertization after operation to extend its life time. The stack operating range of the test bench base configuration without modular extensions is listed in Table 1. Notwithstanding the configuration described above, the control concepts can be adapted individually by the user.

The test bench can be operated manually (every single actuator), partly automated (with individually selectable controllers) or fully automated following a predefined test protocol. Manual interventions by switching controllers on or off or by manipulating the set points or the actuator signals is always possible. Besides the automated transition between the single test points, the test bench operation includes fully automated protecting start up and shut down procedures. Prior to operation, all sensor signals are checked for plausibility, and all actuators are checked for functionality, e.g. by comparing measured pressure losses across certain components with set values. The safety concept includes continuous monitoring of the operation and the initiation of appropriate countermeasures or shut down measures in the event of a malfunction. Limits can be defined individually for each test object. The automation was created using the platform “Morphee” of STS [40].

For membrane humidifier tests, the cathode air conditioning unit is used to provide the humid feed gas. The dry permeate gas is provided by an additional device that uses a mass flow controller and a heat exchanger conditioned with the coolant otherwise supplied to the stack during stack tests. This way, with mainly available components, the permeate inlet temperature is controlled analogously to the principle of the cathode air temperature control. A membrane humidifier test protocol is included in the automation system.

The merging of the two exhaust lines upstream of the throttle ensures the equality of the pressure levels on the feed and the permeate side. An additional throttle in the permeate flow upstream of the merge allows an overpressure of the permeate to the feed side to simulate the pressure losses across the fuel cell stack. This set up enables the decoupled control of pressure level and pressure difference and eliminates the need for synchronization of two pressure controllers, which would otherwise be necessary to limit the pressure difference across the membrane in transient operating points.

The relative humidity is measured by two sensors, the Vaisala HMT310FC and the $E+E$ EE33, with the results of both sensors agreeing well. Both sensors measure the relative humidity and are heated to prevent condensation on the sensor element. Potential amounts of liquid water cannot be detected using this set up. However, the areas of saturation are not reached in the experiments presented in the next chapter.

Table 1
Operating range of the base test bench without extensions.

Parameter	Unit	Operating range
Stack power	kW	2…40
Stack voltage	V	0…200
Electric current	A	0…420
Test object inlet temperature	°C	15…85
Test object inlet pressure	bar(a)	1…4
Relative inlet humidity	%	5…99
Coolant inlet temperature	°C	20…95

4. Experiments

On the test bench, two hollow-fiber membrane humidifiers were tested: the Fumatech H10N, see Fig. 3, denoted as “Humidifier A” in the following, contains a bundle of around 1600 tubes, each with a diameter of 1 mm and a length of 240 mm. In order to approximate the behavior of larger humidifiers, whose bundles insulate each other, the test object is insulated with a 10 mm foam jacket. The humidifier and the immediate sensor region were fully insulated to minimize parasitic heat losses. Outlet humidity was measured directly at the device outlet, ensuring that no downstream thermal effects influenced the recorded humidity values. The second humidifier tested is that of the Hyundai Nexo, denoted as “Humidifier B”, see Fig. 4, and contains three bundles in total with 2.9 times as many tubes of the same length as Humidifier A. The two units were selected because they were readily available for detailed testing and, importantly, because the Hyundai Nexo humidifier represents a state-of-the-art automotive benchmark. This combination provides both a generic commercial reference (Humidifier A) and a system-relevant production component (Humidifier B).

The independent control variables are the mass flow rate of the dry gas, the temperature, the pressure and the relative humidity at the feed inlet, the mass flow rate and the temperature at the permeate inlet as well as the overpressure between permeate and feed inlet. The ranges of variation are listed in Table 2. These operating ranges closely match those encountered in automotive PEM fuel cell systems. The mass flows, pressures, temperatures, and humidity levels in Table 2 therefore represent realistic boundary conditions for stack-level cathode air paths, including both part-load and high-load operation. As test object response, the pressure loss, the temperature and the relative humidity are measured at both the permeate and the feed outlets. The relative humidity at the permeate outlet is the only characteristic value for the humidifier performance measured directly, whereas all other characteristic values, such as dew point approach temperature, the water transfer mass flow rate as well as the water recovery ratio are calculated on this basis.

The test points are recorded fully automatically with adaptive measurement time. Once the current test point is considered stationary, conditioning of the next point is initiated. This is the case when all control variables have been within a tolerance range around the respective set points for 420 s and the test object responses do not exceed predefined spreads for 300 s. Tolerance ranges and spreads, specified in Table 2, are significantly wider than the control quality of the test bench for a robust fully automated test execution. This ensures that all independent variables remained tightly controlled around their set points during each measurement. The dependent variables were recorded only after their temporal variation fell within the defined stability criteria, guaranteeing clear and reproducible boundary conditions. The mass

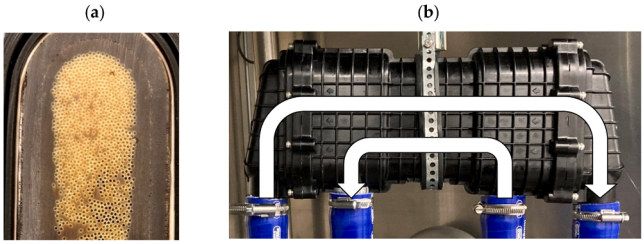

Fig. 3. Humidifier A; Frontal view onto the tube endings with open fluid flow distributor and side view with schematic direction of the fluid flows.

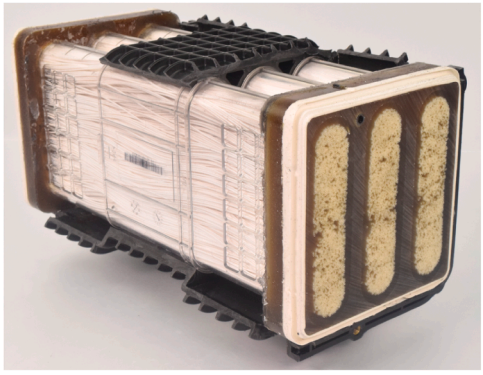

Fig. 4. Humidifier B (cut open) without fluid flow distributor on the permeate side [41]. The feed flow is divided into three parallel bundles and streams along the outside of the thin tubes.

Table 2
Range of variation of the control variables as well as tolerance range and spreads for the fully automated definition of a stationary state.

Control variable	Range of variation	Tolerance range around set point	Test object response	Spread
Dry feed mass flow rate	12 %…100 % $\dot{m}_{max}$	± (0.2 g/s + 1.5 %)	Feed outlet humidity	2 % r. h.
Dry permeate mass flow rate	12 %…100 % $\dot{m}_{max}$	± (0.2 g/s + 1.5 %)	Permeate outlet humidity	2 % r. h.
Feed inlet temperature	40 °C…80 °C	± 1 K	Feed outlet temperature	1.5 K
Permeate inlet temperature	40 °C…80 °C	± 1 K	Permeate outlet temperature	1.5 K
Feed inlet humidity	40 %…98 %	± 1.5 %	Feed pressure loss	-
Feed inlet pressure	1.2 bar(a)… 2.8 bar(a)	± 0.05 bar	Permeate pressure loss	-

flow rate values given in this article are for the dry gas without humidity content.

Due to the higher compactness of Humidifier B, its mass flow specific heat losses to the environment are lower and result in higher outlet temperatures. Since the gas temperatures at the inlet of the downstream components depend strongly on the design conditions in the fuel cell system, they are far less interesting and less relevant than the transferred water masses. As shown in Fig. 5 using selected series of measurements, the results of both humidifiers are well comparable. Systematic deviations are undetectable. Although dedicated repeatability tests were not carried out, the close agreement between the two structurally different humidifiers across the full operating range indicates a high level of reproducibility and supports the robustness of the reported trends. For direct comparability, the transferred water masses and air flow rates in this article are related to the number of tubes of Humidifier A, i.e. the corresponding quantities for Humidifier B are 2.9 times as large.

A total of 748 test points were recorded for Humidifier A and 497 test points for Humidifier B. While most of the control variables in Table 2 were varied completely independently of each other, there is a certain degree of dependence between the feed and permeate inlet temperatures (see Fig. 6b). Since large temperature differences between feed and permeate inlet temperatures do not seem to be practicable in fuel cell system applications, these combinations are not considered in order to reduce the number of test points or to increase the accuracy in more relevant areas. Considering the relatively slow dynamic behavior of the temperature compared with other parameters, it is only varied in discrete values, which, in combination with the grouping of points of the same temperatures into blocks, enables a time efficient execution of the measurement program.

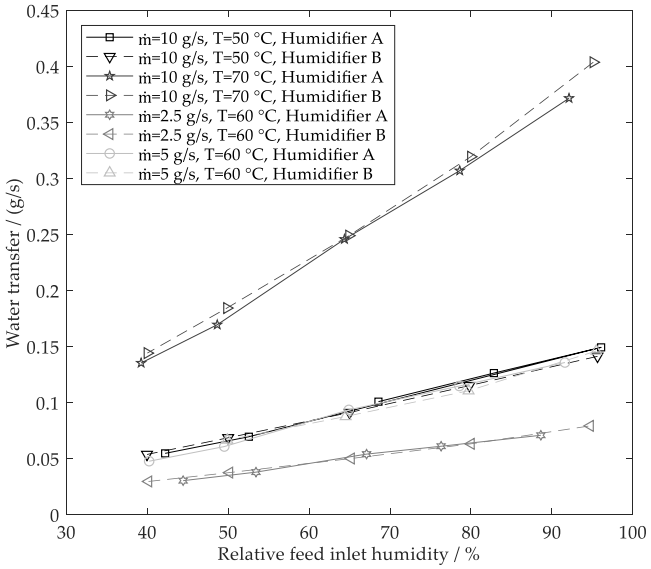

Fig. 5. Comparison of the humidification performance of Humidifier A and Humidifier B; all mass flow rates $\dot{m}$=$\dot{m}_{dr}$, feed=$\dot{m}_{dr}$, permeate referenced to the number of tubes of Humidifier A, pressure level at permeate and feed inlet $p = 2$ bar(a), $T_{permeate\ in} = T_{feed\ in}$, dry gas at the permeate inlet.

The minimum possible mass flow rate that allows a variation of the gas temperature and feed humidity in the relevant ranges is about $\dot{m}_{dr,Feed,min} = 2.5$ g/s. For the larger Humidifier B, this corresponds to a lower mass flow rate relative to the number of tubes of Humidifier A. Taking advantage of this circumstance, minimum mass flow rates of 1.2 g/s relative to the number of tubes of Humidifier A are investigated with Humidifier B, thus extending the operating range for low part load operating points or high bypass rates (see Fig. 6a).

5. Regression model

Based on the measurement data of the two humidifiers, a correlation model using Gaussian Process Regression (GPR) is created with the tool xCal by STS. Because all operating points were reached under quasi-stationary conditions, transient membrane dynamics were not included; their influence is expected to be small. The combined dataset of > 1200 test points exceeds the recommended minimum size for this type of multiparametric xCal correlation by roughly one order of magnitude. This extensive coverage contributes directly to the robustness of the resulting GPR model. The model quality is presented in the following.

GPR was chosen for several reasons that align closely with the characteristics of the present dataset and the physical behavior of membrane humidifiers. First, GPR is a non-parametric method whose complexity grows with the available data, avoiding restrictive functional forms that often fail to capture the coupled nonlinear effects observed in full-scale humidifiers. Second, GPR typically performs strongly on small to medium-sized datasets, in contrast to deep learning or ensemble methods that require substantially larger training sets to generalize reliably. Third, the kernel formulation allows imposing smoothness priors and interpreting correlations in a physically meaningful way. Unlike polynomial fits, GPR avoids oscillatory artifacts, and unlike tree-based models it ensures continuity and differentiability of the predicted surfaces. Finally, GPR includes an explicit noise term, allowing systematic treatment of experimental variability and sensor uncertainty. These characteristics make GPR particularly well suited for the present correlation task.

The measured relative humidity as such is no suitable characteristic value due to its strong dependence on the temperature. Instead, the transferred water mass flow is used due to the good match between both

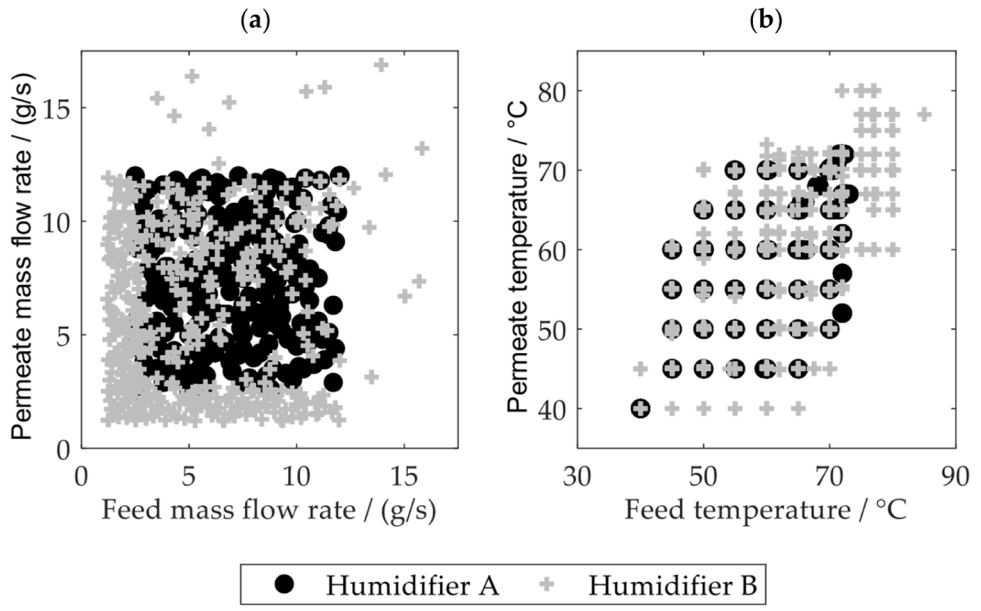

Fig. 6. Dependencies of feed and permeate mass flow rates (left), referenced to the number of tubes of Humidifier A; feed and permeate temperature (right) for all test points of Humidifier A and Humidifier B.

humidifier types with the same number of tubes. Since Humidifier B provides better temperature results for the reasons mentioned above, only the measurement points of Humidifier B, which cover a wider temperature range, are used for the correlation model to predict the permeate and feed outlet temperatures.

The model quality is good with a coefficient of determination for the training points $R^2_{Training} > 98$ % and for the validation points $R^2_{Val} > 99$ %. The root mean squared deviation (RMSD) is approx. RMSD = 0.01 g/s (see Table 3). The model quality for the temperatures is even better with a coefficient of determination for the training points $R^2_{Training} > 99$ %. This is due to the lower complexity resulting from the dependence of significantly fewer variables, as well as the higher measurement accuracy of the temperatures compared to the dew points. Additionally, the root mean squared deviation is very low for the training points $RMSD_{Training} < 0.4$ K as well as for the validation points $RMSD_{Val} < 0.6$. This is reflected in Fig. 7, where the predicted values are compared with the measured ones for each training and validation point. A detailed uncertainty quantification could provide additional insight, but was not the focus of this study. Because GPR explicitly models measurement noise, random sensor uncertainties are naturally smoothed within the regression process; nevertheless, extended uncertainty analysis remains a valuable direction for future work. All model predictions shown in this work remain strictly within the experimentally measured input space, so no extrapolation is performed. While GPR can in principle overfit, the large dataset and the inherent noise modeling reduce this risk; nonetheless, the method's limitations outside the measured range are acknowledged.

6. Parameter influence

Since statistical inaccuracies are compensated and the unchanged parameters remain constant, this section demonstrates the influence of the selected parameters using the results of the correlation model. Each phenomenon presented is also visible in the measurement data directly.

Influence of the relative humidity. As exemplarily shown in Fig. 8a for an inlet temperature level $T = 60$ °C on both sides, pressures $p = 2$ bar(a) and four mass flow rates, the permeate outlet humidity increases with increasing feed inlet humidity. The water recovery ratio (see Fig. 8b) increases by several percentage points with increasing relative feed inlet humidities between 50 % and 80 %, whereas it is rather constant at humidities above and below. Higher humidity therefore enables a disproportionally higher, and therefore more effective, water transfer in relation to the feed water provided.

These observed increased water transfer rates with higher feed inlet humidities can be explained with the molecular structure of the membrane, which is expected to be similar to that of common polymer electrolyte membranes. This is in accordance with an improved water transfer with higher membrane humidities (compare [42]).

In fact, permeate outlet humidities of 50 % maximum may appear small for fuel cell operation. It should be noted, however, that in preferred operating points of a fuel cell system, the feed inlet humidity is approximately 100 %. In case the permeate outlet humidity is related to the temperature of the coolant at stack inlet – often > 10 K below the temperature at the stack outlet – the relative humidity is significantly higher. In a simplified approach, as can be seen in the additional curves in Fig. 8a, the permeate outlet humidity is related to a temperature 10 K below the permeate outlet temperature leading to maximum relative humidities between 65 % and 82 %. As explained in one of the subsequent sections, a lower permeate inlet temperature also results in a higher water transfer, which, however, is not taken into account in this specific simplified context.

Mass flow rate influence. Permeate and feed mass flow rates significantly affect the humidification performance, as shown in Fig. 9 for otherwise constant conditions with inlet temperatures $T = 60$ °C on both

Table 3
Quality of the correlation models for water transfer, feed and permeate outlet temperatures of the membrane humidifiers.

Model	Number of training points	Number of validation points	$R^2_{Training}$	R^2_{Val}	$RMSD_{Training}$	$RMSD_{Val}$
Water transfer	1205	40	0.9873	0.9908	0.0125 g/s	0.0107 g/s
Feed outlet temperature	473	24	0.9982	0.9964	0.3431 K	0.4735 K
Permeate outlet temperature	473	24	0.9983	0.9956	0.3465 K	0.5698 K

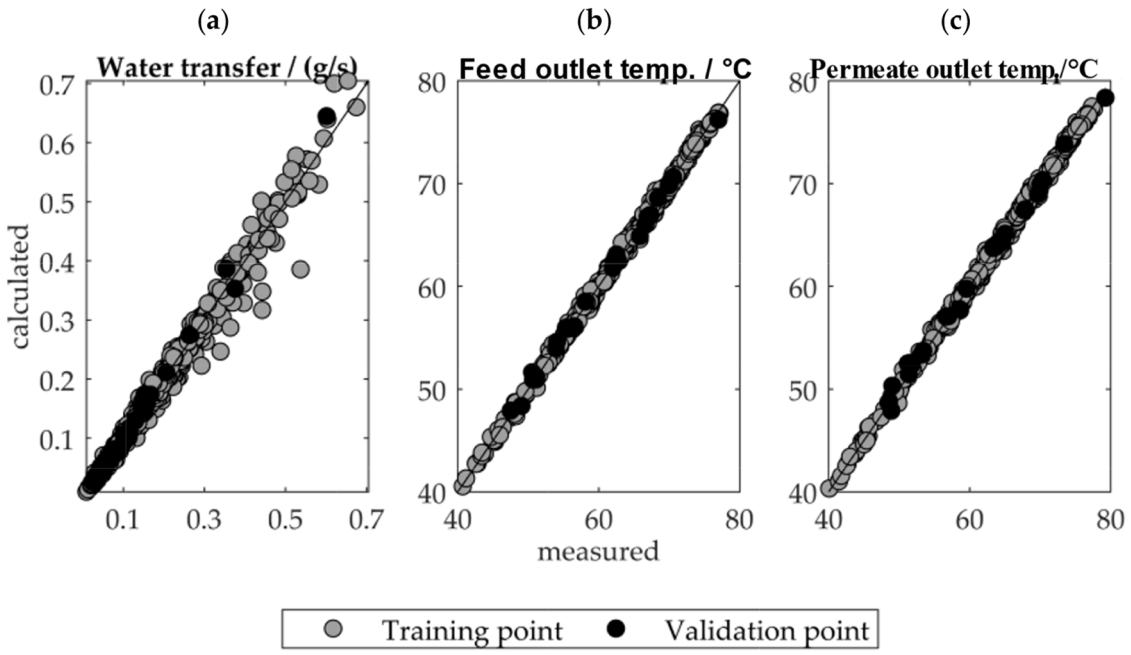

Fig. 7. Model accuracy for the transferred water mass flow rate referenced to the number of tubes of Humidifier A (left), as well as for the feed (center) and the permeate outlet temperature (right).

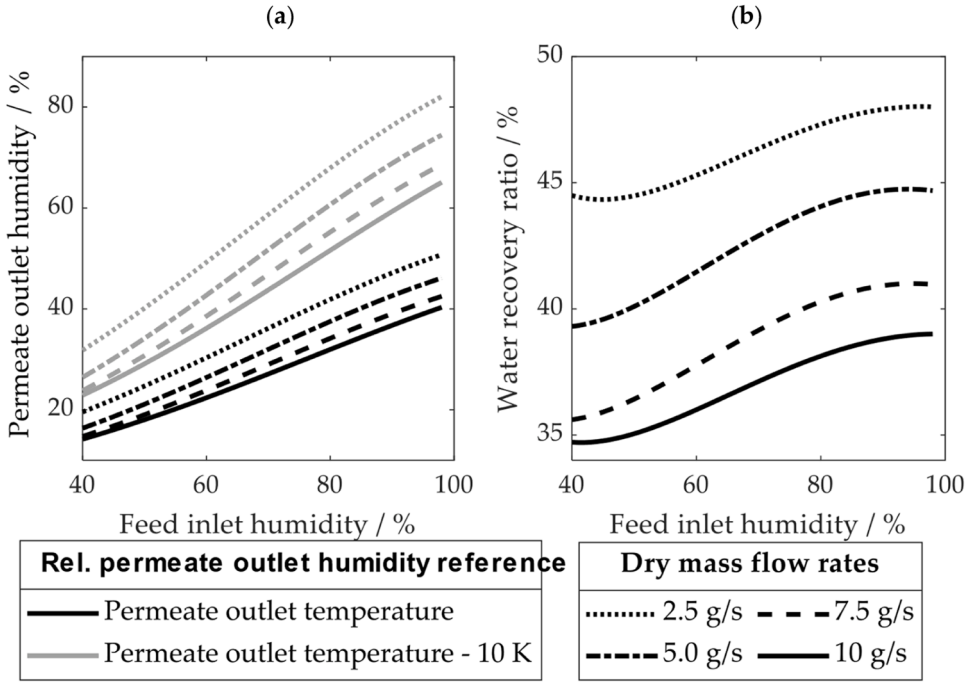

Fig. 8. Influence of the relative feed inlet humidity on the permeate outlet humidity and the water recovery ratio for several dry gas mass flow rates $\dot{m}_{dr,feed} = \dot{m}_{dr,permeate}$, referenced to the number of tubes of Humidifier A, with constant fluid inlet temperatures $T_{feed,in} = T_{permeate,in} = 60\ °C$, dry gas at the permeate inlet and a pressure level $p = 2$ bar on feed and permeate side.

sides, pressures $p = 2$ bar and relative feed inlet humidity $\varphi_{Feed,in} = 92$ %. The dashed line marks the correlation between dry feed and permeate mass flow rates for a cathode stoichiometry $\lambda_{O2} = 2$ (referred to as operating line in the following) taking into account the oxygen consumption. All mass flow rates are for the dry gases without water content.

Along the operating line, the permeate outlet humidity moderately decreases with increasing mass flow rates. Increasing feed or permeate flow rates show contrary effects. An increase of the feed flow rate results in a strong increase of the permeate outlet humidity. A higher permeate mass flow with constant feed mass flow rate, however, leads to a significant decrease of the relative permeate outlet humidity.

This is because a higher feed mass flow rate results in a higher humidity along the channels and thus a higher driving potential. Although a higher permeate mass flow rate also increases the driving potential, the higher permeate mass flow rate predominates, which leads to a lower specific water uptake.

An increasing feed as well as permeate mass flow rate lead to an

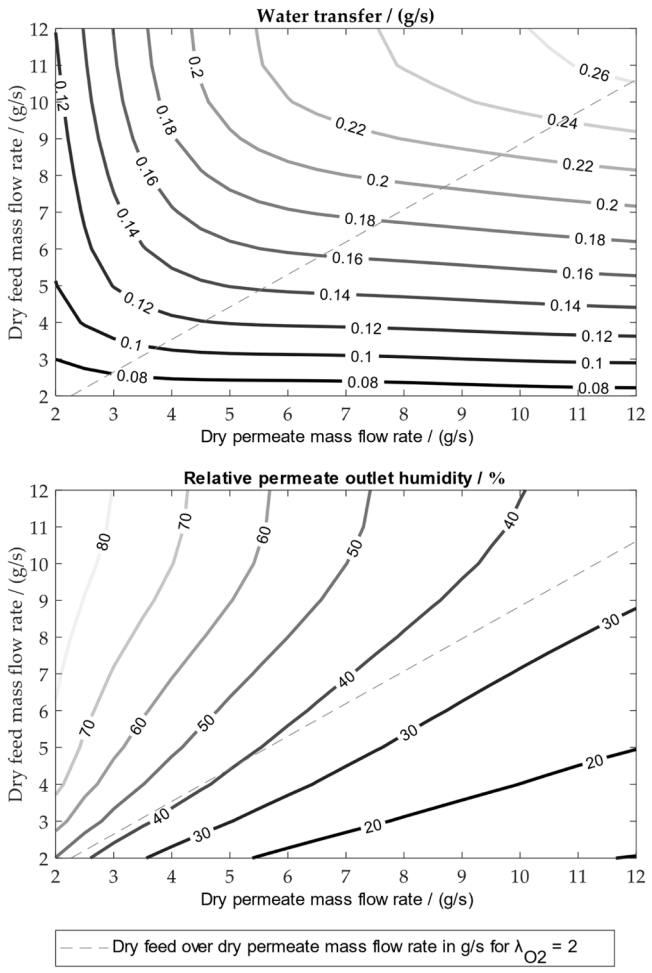

Fig. 9. Absolute water transfer and relative permeate outlet humidity depending on the dry mass flow rates on feed and permeate sides, both referenced to the number of tubes of Humidifier A, with constant fluid inlet temperatures $T = 60$ °C, pressure level $p = 2$ bar(a) on feed and permeate sides, dry gas at permeate inlet and a relative feed inlet humidity $\varphi_{\text{feed in}} = 92$ %.

increasing water transfer. The influence of the feed flow rate is significantly more distinct than that of the permeate mass flow rate. While, based on a combination of a dry permeate mass flow rate $\dot{m}_{\text{dr,permeate}} = 8$ g/s and a dry feed mass flow rate $\dot{m}_{\text{dr,Feed}} = 7$ g/s on the operating line, halving the feed mass flow rate leads to a reduction in water transfer by 40 %, reducing the permeate mass flow rate in the same ratio with constant feed mass flow rate leads to a reduction in water transfer by only 15 %.

This can be explained as follows. Reducing the permeate mass flow rate leads to an increased relative permeate outlet humidity and humidity ratio of the reduced permeate flow. Consequently, the absolute water mass transfer hardly decreases in large areas. In contrast, a reduction of the feed mass flow rate directly reduces the water supply resulting in a substantial water mass transfer reduction.

This insight allows important conclusions for the fuel cell system topology. In order to reduce the cathode inlet humidity, part of the mass flow can be bypassed around the permeate or feed side and mixed afterwards with the respective partial flow through the humidifier. In this case, the absolute value of the relative humidity is determined by the absolute water transfer. Against the background described above, a bypass around the feed side is much more effective than around the permeate side. Furthermore, the control of the bypass ratio is much more robust due to the almost linear correlation between the reduction of the feed mass flow rate and the reduction of the transferred water.

This configuration is also beneficial when starting up and shutting down. A bypass on the permeate side can lead to an undesirable accumulation of liquid water on the permeate side during phases of low or no mass flow through the permeate tubes, which is fed to the stack in the form of larger droplets with subsequently increasing mass flow rates. This liquid water accumulation can be prevented by locating the bypass on the feed instead of permeate side. For safe cold start procedures, prior drying of both the stack and the membrane humidifier is essential. A bypass on the feed side enables drying not only of the cathode supply air, but also of the membrane humidifier itself.

Temperature influence. In fuel cell system applications, permeate and feed inlet temperatures are usually not identical – as in the above considerations – but depend on the charge air cooler and its integration into the cooling circuit as well as on the stack operating parameters coolant inlet temperature and temperature spread. Furthermore, the humidifier inlet temperatures could potentially be varied as independent variables.

In order to understand the influence of the respective temperatures on the humidification performance the first step is to analyze the correlation between inlet and outlet temperatures. Fig. 10 shows the feed and permeate outlet temperatures as functions of the permeate inlet temperature for four different feed inlet temperatures with otherwise constant parameters.

Whereas identical fluid inlet temperatures at a low temperature level entail only marginally lower outlet temperatures (against the background of the ambient temperature of approx. 32 °C), with higher fluid inlet temperatures a higher temperature and heat loss to the environment can be observed.

The permeate outlet temperature correlates positively with the permeate as well as the feed inlet temperature, with the correlation being stronger with the latter. Analogously, the feed outlet temperature correlates positively with both inlet temperatures, but here the correlation with the permeate inlet temperature is stronger.

The stronger influence on the respective other outlet temperature originates from the countercurrent fluid flow. This correlation, as shown in the following, is relevant because of its influence on the water transfer. At the same time, due to the still significant influence of the inlet temperature on the outlet temperature of the respective same side, it can be stated that the humidifiers are not ideal heat exchangers.

In Fig. 11 the influence of feed and permeate inlet temperatures on

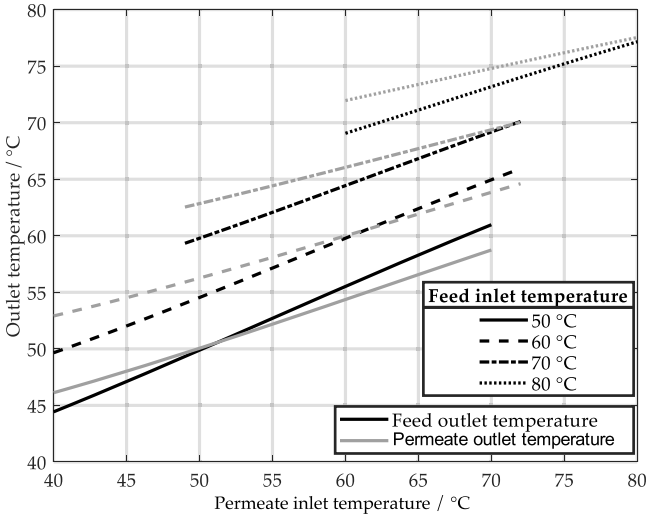

Fig. 10. Permeate and Feed outlet temperatures depending on the permeate inlet temperature for four different feed inlet temperatures with constant flow rates of the dry gas on feed and permeate sides $\dot{m}_{\text{dr,feed}} = \dot{m}_{\text{dr,permeate}} = 5$ g/s, referenced on the number of tubes of Humidifier A, a pressure level $p = 2$ bar(a) on feed and permeate sides, dry gas at the permeate inlet and relative feed inlet humidity
$\varphi_{\text{feed,in}} = 95$ %.

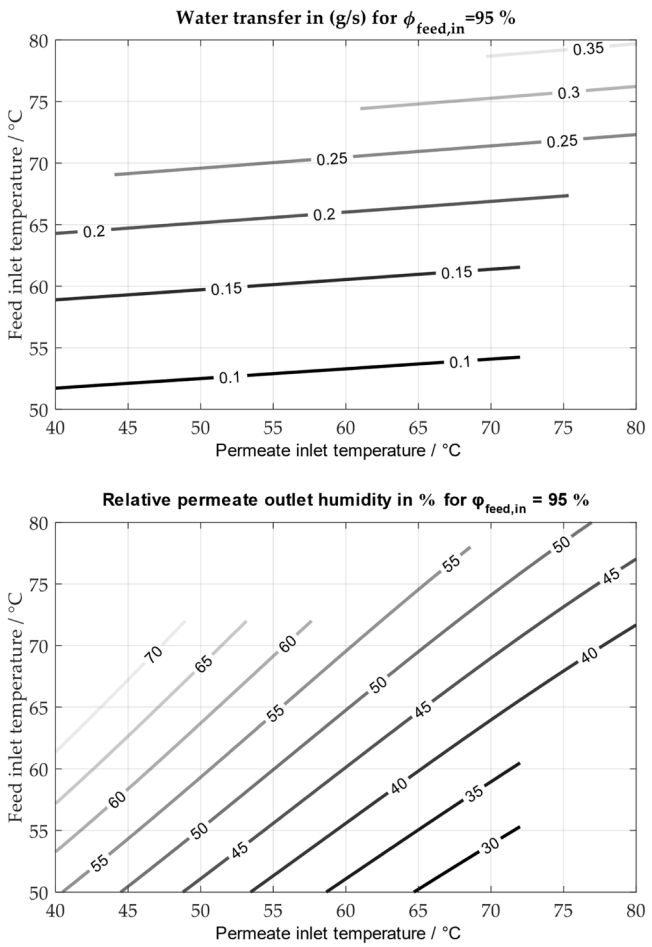

Fig. 11. Absolute water transfer and relative permeate outlet humidity depending on feed and permeate inlet temperature with constant dry feed and permeate mass flow rates $\dot{m}_{dr,feed} = \dot{m}_{dr,permeate} = 5$ g/s, referenced to the number of tubes of Humidifier A, pressure level $p = 2$ bar on the feed and permeate sides, dry gas at the permeate inlet and relative feed inlet humidity $\varphi_{feed,in} = 95$ %.

the water transfer and on the relative permeate outlet humidity is depicted. With evenly increasing feed and permeate inlet temperatures, the relative permeate outlet humidity remains nearly constant. Feed and permeate inlet temperatures have contrary effects on the water transfer and the relative permeate outlet humidity.

With increasing permeate and constant inlet temperature, the observed decrease of the relative permeate outlet humidity is to be expected due to the increasing permeate outlet temperature. At first glance, a higher absolute water transfer might be expected. Given the stronger influence of the permeate inlet temperature on the feed than on the permeate outlet temperature due to the counterflow arrangement, a slight decrease in water transfer is observed instead, while more water leaves the humidifier on the feed side.

With increasing feed and constant permeate inlet temperature, at constant relative feed inlet humidities and comparable water recovery ratios, the water transfer rate increases solely because of the higher feed water quantities. In consequence, the relative permeate outlet humidity rises as well.

For fuel cell systems, the influence of the permeate inlet temperature is particularly relevant; in simple system configurations, the permeate inlet temperature depends on the coolant stack inlet temperature but can potentially also be controlled independently. While in many systems a charge air cooler is installed upstream of the membrane humidifier on the permeate side, through which coolant flows at stack inlet temperature, the permeate temperature level could be raised relatively easily by using the coolant from the stack outlet due to the temperature rise in the stack. Given the increased water transfer at lower permeate temperatures, these options are rather unprofitable. The feed inlet temperature, however, mainly depends on the coolant temperature spread across the stack and cannot be influenced independently without additional components.

In order to decouple the influence of the temperature from the correlating absolute feed inlet water content, the influence of feed temperature and dewpoint on the water mass transfer and the relative permeate outlet humidity is considered in Fig. 12. At constant pressure, the absolute water content is determined by the dew point. Liquid water at the feed inlet with dew point above the dry bulb temperature is not considered. The permeate inlet temperature corresponds to the dew point temperature of the feed inlet. Additionally, the relative feed inlet humidity is plotted.

With constant dew point, an increasing feed inlet temperature comes along with a lower relative feed inlet humidity. Although the temperature at the permeate increases more than at the feed outlet and thus the relative humidity at the permeate outlet decreases, the overall water transfer decreases slightly. This corresponds well to the observations described above, which indicate more effective water transfer with higher relative humidity. In general, strong temperature-independent

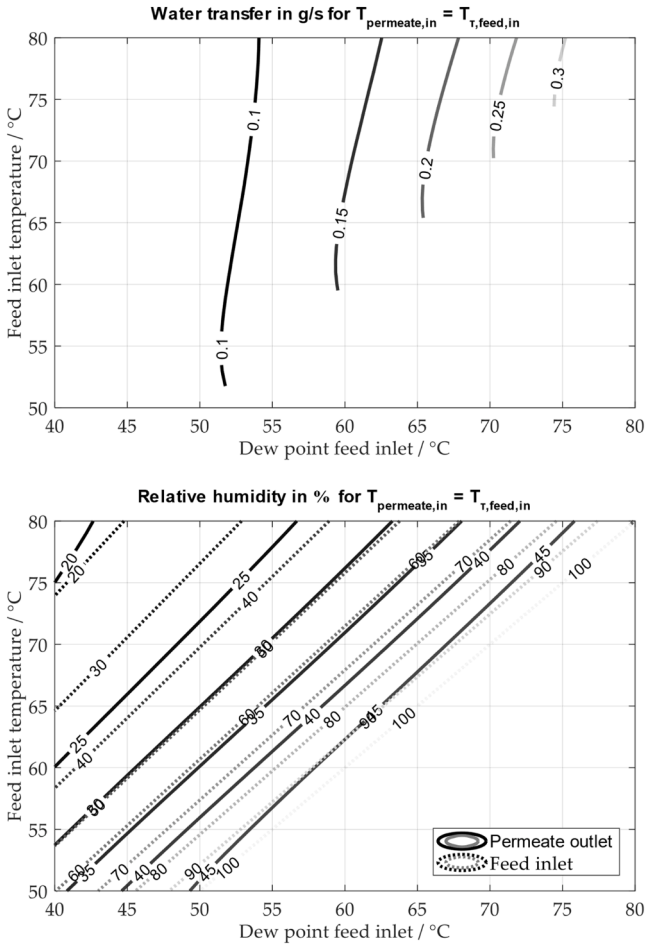

Fig. 12. Absolute water transfer and relative permeate outlet humidity depending on dry bulb and dew point temperature of the feed inlet with constant dry feed and permeate mass flow rates $\dot{m}_{dr,feed} = \dot{m}_{dr,permeate} = 5$ g/s, referenced to the number of tubes of Humidifier A, pressure level $p = 2$ bar on feed and permeate sides, and dry gas at the permeate inlet. The permeate inlet temperature equals the dew point temperature of the feed inlet. For orientation, the relative feed inlet humidity is plotted additionally.

correlations of the permeate outlet humidity with the feed inlet humidity can be observed.

Differential pressure influence. In a fuel cell system, the cathode exhaust gas flows through the feed side and the dry cathode supply gas is passed through the permeate side. The pressure loss across the stack results in a differential overpressure of the permeate to the feed side, which increases with increasing cathode mass flow rate.

While the previous variations are subject to overpressures well below 100 mbar, the influence of larger overpressures is analyzed separately below. As exemplarily shown in Fig. 13 for a dry mass flow rate $\dot{m}_{dr,permeate} = \dot{m}_{dr,feed} =$ 7,5 g/s, no distinct influence of the pressure difference across the membrane on the water transfer rate can be detected. 110 dedicated measurement points with systematically varied differential pressures, none of which exhibited a measurable effect on the transferred water mass, support this conclusion. The absence of any detectable trend across these tests provides strong experimental confirmation of the negligible influence of pressure difference. The same applies to other mass flow rates.

The measurements of Humidifier B confirm the independence of the absolute water transfer from the differential pressure across the membrane at various feed inlet humidities, temperature levels, feed pressures and mass flow rates. This independence also applies to different dry feed mass flow rates, when these are reduced compared to the permeate mass flow rate, as is the case when using a bypass.

The higher permeate pressure in real applications in combination with the same absolute water transfer rate leads to higher permeate outlet humidities than in the previous single parameter variations, which is advantageous for the operation and dimensioning of the humidifier.

As a consequence of this finding, apart from 57 test points for Humidifier A and 53 for Humidifier B, which were subject to differential pressure, neither a specific variation of the pressure difference across the membrane was experimentally carried out nor a corresponding parameter was included in the GPR models.

7. Conclusion

Membrane humidifiers are essential components in PEM fuel cell systems, yet their behavior under realistic operating conditions is insufficiently documented in the literature. This work addresses this gap by experimentally characterizing two full-scale gas-to-gas membrane humidifiers across a wide and application-relevant parameter space. In contrast to most previous studies, which focus on single membranes or simplified boundary conditions, the present investigation provides comprehensive data for complete humidifier modules under realistic thermal, pressure, and flow conditions.

Based on $>$ 1200 high-fidelity measurement points, a data-driven correlation model using Gaussian Process Regression was developed. The model accurately predicts water transfer and outlet temperatures and thus represents a novel, validated tool for system-level fuel cell simulations. Although the focus of this work is not a mechanistic analysis, the resulting correlations capture the combined heat and mass transfer behavior of full-scale humidifiers more comprehensively than existing simplified models. They thereby provide a robust empirical foundation for future studies aimed at deeper physical interpretation. The analysis of the parameter influence reveals several previously unreported insights with direct implications for system design:

1. Feed-side bypassing provides nearly linear and robust control of water transfer and enables efficient drying during shutdown.
2. High permeate-side inlet temperatures significantly reduce humidification performance.
3. Differential pressure across the membrane has no measurable effect on water transfer, which reduces the number of relevant operating variables for future experiments and models.

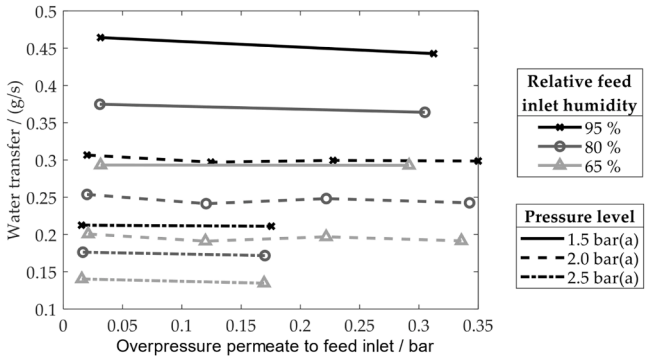

Fig. 13. Influence of the overpressure of the permeate to the feed inlet on the water transfer rate for Humidifier A for various feed inlet pressure levels and feed inlet humidities with constant dry mass flow rates $\dot{m}_{dr,feed} = \dot{m}_{dr,permeate} =$ 7.5 g/s, dry gas at permeate inlet and temperatures $T_{feed,in} = T_{permeate,in} =$ 70 °C.

Overall, this study provides both the most extensive experimental dataset for automotive-scale membrane humidifiers published to date and a validated correlation model for integration into fuel cell system simulations. These contributions offer a solid foundation for improved system topology design, operating strategies, and modeling approaches, thereby advancing the development of efficient and reliable PEM fuel cell systems. The resulting design and operation guidelines reflect general humidification principles and are therefore applicable across a wide range of fuel cell system architectures. While specific layouts may require adaptation, the underlying trends and recommended measures remain broadly valid.

CRediT authorship contribution statement

Sören Tinz: Writing – original draft, Funding acquisition, Formal analysis, Conceptualization. **Julian Toussaint:** Writing – original draft, Visualization, Validation. **Maximilian Schmitz:** Writing – review & editing, Methodology, Data curation. **Marius Walters:** Writing – review & editing, Writing – original draft, Resources, Project administration. **Stefan Pischinger:** Writing – review & editing, Project administration, Funding acquisition.

Declaration of competing interest

The authors declare that they have no known competing financial interests or personal relationships that could have appeared to influence the work reported in this paper.

Acknowledgments

This work was funded by the Deutsche Forschungsgemeinschaft (DFG, German Research Foundation) – GRK 1856

Data availability

Data will be made available on request.

References

[1] T.A. Zawodzinski, T.E. Springer, J. Davey, R. Jestel, C. Lopez, J. Valerio, S. Gottesfeld, A comparative study of water uptake by and transport through ionomeric fuel cell membranes, J. Electrochem. Soc. 140-7 (1993) 1981–1985.
[2] T. Yoshizumi, H. Kubo, M. Okumura, Development of high-performance FC stack for the new MIRAI, SAE Tech. Pap. (2021), https://doi.org/10.4271/2021-01-0740.
[3] M. Walters, M. Wick, S. Tinz, J. Ogrzewalla, A. Sehr, S. Pischinger, SAE Int. J. Alt. Power (2018) 3, https://doi.org/10.4271/2018-01-1305.
[4] S. Tinz, S. Dirkes, M. Walters, J. Andert, Fuel cells, in: B. Elvers, A. Schütze (Eds.), Handbook of Fuels, Publisher: Wiley-VCH, 2022, pp. 447–464.

[5] S. Park, I.-H. Oh, An analytical model of Nafion™ membrane humidifier for proton exchange membrane fuel cells, J. Power. Sources. 2 (2009) 498–501, https://doi.org/10.1016/j.jpowsour.2008.12.018.
[6] S. Kang, K. Min, S. Yu, Two-dimensional dynamic modeling of a shell-and-tube water-to-gas membrane humidifier for proton exchange membrane fuel cell, Int. J. Hydrogen. Energy 4 (2010) 1727–1741, https://doi.org/10.1016/j.ijhydene.2009.11.105.
[7] D. Chen, W. Li, H. Peng, An experimental study and model validation of a membrane humidifier for PEM fuel cell humidification control, J. Power. Sources. 1 (2008) 461–467, https://doi.org/10.1016/j.jpowsour.2008.02.055.
[8] S. Kang, K. Min, S. Yu, Dynamic modeling of a proton exchange membrane fuel cell system with a shell-and-tube gas-to-gas membrane humidifier, Int. J. Hydrogen. Energy 7 (2012) 5866–5875, https://doi.org/10.1016/j.ijhydene.2011.12.063.
[9] C.-Y Chen, W.-M Yan, C.-N Lai, J.-H. Su, Heat and mass transfer of a planar membrane humidifier for proton exchange membrane fuel cell, Int. J. Heat. Mass Transf. (2017) 601–608, https://doi.org/10.1016/j.ijheatmasstransfer.2017.02.045.
[10] M. Solsona, C. Kunusch, C. Ocampo-Martinez, Control-oriented model of a membrane humidifier for fuel cell applications, Energy Convers. Manage (2017) 121–129, https://doi.org/10.1016/j.enconman.2017.01.036.
[11] R.K. Ahluwalia, X. Wang, W.B. Johnson, F. Berg, D. Kadylak, Performance of a cross-flow humidifier with a high flux water vapor transport membrane, J. Power. Sources. (2015) 225–238, https://doi.org/10.1016/j.jpowsour.2015.05.013.
[12] S.-K Park, S.-Y Choe, S. Choi, Dynamic modeling and analysis of a shell-and-tube type gas-to-gas membrane humidifier for PEM fuel cell applications, Int. J. Hydrogen. Energy 9 (2008) 2273–2282, https://doi.org/10.1016/j.ijhydene.2008.02.058.
[13] R. Huizing, M. Fowler, W. Mérida, J. Dean, Design methodology for membrane-based plate-and-frame fuel cell humidifiers, J. Power. Sources. 1 (2008) 265–275, https://doi.org/10.1016/j.jpowsour.2008.01.046.
[14] B.-B Wang, W.-K Li, C.-Y Lee, W.-M Yan, M. Ghalambaz, A novel geometrical design of gas-to-gas planar membrane humidifier for proton electrolyte membrane fuel cells, Int. J. Energy Res. 1 (2021) 83, https://doi.org/10.1002/er.6854.
[15] S.Z. Hashemi-Valikboni, S.S.M. Ajarostaghi, M.A. Delavar, K. Sedighi, Numerical prediction of humidification process in planar porous membrane humidifier of a PEM fuel cell system to evaluate the effects of operating and geometrical parameters, J. Therm. Anal. Calorim. 5 (2020) 1687–1701, https://doi.org/10.1007/s10973-020-10058-6.
[16] E. Afshari, N.B. Houreh, Two-dimensional numerical modeling of a membrane humidifier with porous media flow field for PEM fuel cell, Int. J. Mod. Phys. C. 06 (2015) 1550061, https://doi.org/10.1142/S0129183115500618.
[17] D. Kadylak, P. Cave, W. Mérida, Effectiveness correlations for heat and mass transfer in membrane humidifiers, Int. J. Heat. Mass Transf. 5-6 (2009) 1504–1509, https://doi.org/10.1016/j.ijheatmasstransfer.2008.09.002.
[18] W.-M Yan, C.-Y Lee, C.-H Li, W.-K Li, S. Rashidi, Study on heat and mass transfer of a planar membrane humidifier for PEM fuel cell, Int. J. Heat. Mass Transf. (2020) 119538, https://doi.org/10.1016/j.ijheatmasstransfer.2020.119538.
[19] N.B. Houreh, E. Afshari, Three-dimensional CFD modeling of a planar membrane humidifier for PEM fuel cell systems, Int. J. Hydrogen. Energy 27 (2014) 14969–14979, https://doi.org/10.1016/j.ijhydene.2014.07.037.
[20] N.B. Houreh, M. Ghaedamini, H. Shokouhmand, E. Afshari, A.H Ahmaditaba, Experimental study on performance of membrane humidifiers with different configurations and operating conditions for PEM fuel cells, Int. J. Hydrogen. Energy 7 (2020) 4841–4859, https://doi.org/10.1016/j.ijhydene.2019.12.017.
[21] P. Cave, W. Mérida, Water flux in membrane fuel cell humidifiers: flow rate and channel location effects, J. Power. Sources. 1 (2008) 408–418, https://doi.org/10.1016/j.jpowsour.2007.08.103.
[22] D. Kadylak, W. Mérida, Experimental verification of a membrane humidifier model based on the effectiveness method, J. Power. Sources. 10 (2010) 3166–3175, https://doi.org/10.1016/j.jpowsour.2009.12.005.
[23] M.B. Satterfield, J.B. Benziger, Non-Fickian water vapor sorption dynamics by nafion membranes, J. Phys. Chem. B 12 (2008) 3693–3704, https://doi.org/10.1021/jp7103243.
[24] P. Krtil, A. Trojánek, Z. Samec, Kinetics of water sorption in NafionThin films – quartz crystal microbalance study, J. Phys. Chem. B 33 (2001) 7979–7983, https://doi.org/10.1021/jp004162t.
[25] S. Ge, X. Li, B. Yi, I.-M. Hsing, Absorption, desorption, and transport of water in polymer electrolyte membranes for fuel cells, J. Electrochem. Soc. 6 (2005) 1149–1157.
[26] D. McKay, A. Stefanopoulou, J. Cook, A controllable membrane-type humidifier for fuel cell applications—part I: operation, modeling and experimental validation, J. Fuel. Cell Sci. Technol. (2010).
[27] D. McKay, A. Stefanopoulou, J. Cook, A controllable membrane-type humidifier for fuel cell applications—part II: controller design, analysis and implementation, J. Fuel. Cell Sci. Technol. (2011).
[28] T.E. Springer, T.A. Zawodzinski, S. Gottesfeld, Polymer electrolyte fuel cell model, J. Electrochem. Soc. 138 (8) (1991) 2334–2342.
[29] D. Chen, H. Peng, A-thermodynamic-model-of-membrane-humidifiers-for-PEM-fuel-cell-humidification-control, ASME J. Dyn. Syst. Meas. Control (2005) 127.
[30] M. Sabharwal, C. Duelk, D. Bhatia, Two-dimensional modeling of a cross flow plate and frame membrane humidifier for fuel cell applications, J. Memb. Sci. 8 (2012) 285–301, https://doi.org/10.1016/j.memsci.2012.03.066.
[31] T. Cahalan, The Analysis of Membranes For External Humidification of PEM Fuel Cells, Dissertation, first. Auflage, München, 2018.
[32] R. Pandey, A. Lele, Modelling of water-to-gas hollow fiber membrane humidifier, Chem. Eng. Sci. 6 (2018) 955–971, https://doi.org/10.1016/j.ces.2018.08.015.
[33] W.-M Yan, C.-H Li, C.-Y Lee, S. Rashidi, W.-K. Li, Numerical study on heat and mass transfer performance of the planar membrane-based humidifier for PEMFC, Int. J. Heat. Mass Transf. 21-22 (2020) 119918, https://doi.org/10.1016/j.ijheatmasstransfer.2020.119918.
[34] E. Afshari, N.B. Houreh, Performance analysis of a membrane humidifier containing porous metal foam as flow distributor in a PEM fuel cell system, Energy Convers. Manage (2014) 612–621, https://doi.org/10.1016/j.enconman.2014.08.067.
[35] C.-Y Chen, J.-H Su, H.M. Ali, W.-M Yan, M. Amani, Effect of channel structure on the performance of a planar membrane humidifier for proton exchange membrane fuel cell, Int. J. Heat. Mass Transf. 7–8 (2020) 120522, https://doi.org/10.1016/j.ijheatmasstransfer.2020.120522.
[36] W.-M Yan, C.-Y Chen, Y. Jhang, Y.-H Chang, P. Amani, M. Amani, Performance evaluation of a multi-stage plate-type membrane humidifier for proton exchange membrane fuel cell, Energy Convers. Manage (2018) 123–130, https://doi.org/10.1016/j.enconman.2018.09.027.
[37] C.E. Rasmussen, C. Williams (Eds.), Gaussian Processes for Machine Learning, MIT Press, Cambridge, MA, 2006.
[38] E. Schulz, M. Speekenbrink, A. Krause, Tutorial on Gaussian process regression: modelling, exploring, and exploiting functions, J. Math. Psychol. (2018) 1–16.
[39] S. Raman, S. Swaminathan, S. Bhardwaj, H.K. Tanneru, B. Bullecks, R. Rengaswamy, Rapid humidity regulation by mixing of dry and humid gases with feedback control for PEM fuel cells, Int. J. Hydrogen. Energy 1 (2019) 389–407, https://doi.org/10.1016/j.ijhydene.2018.04.187.
[40] FEV Europe GmbH, Neuenhofstr. 181, 52078 Aachen.
[41] Hyundai Nexo Benchmarking, FEV Europe GmbH, Neuenhofstr 181 (2019) 52078. Aachen.
[42] V. Rao, N. Kluy, W. Ju, U. Stimming, Proton-conducting membranes for fuel cells. Handbook of Membrane Separations: Chemical, Pharmaceutical, Food, and Biotechnological Applications; Publisher: CRC Press, Taylor & Francis Group, 2015.